Heliyon 10 (2024) e24075

Contents lists available at ScienceDirect

Heliyon

journal homepage: www.cell.com/heliyon

Research article

Anti-virulence potential of patuletin, a natural flavone, against *Staphylococcus aureus: In vitro* and *In silico* investigations

Ahmed M. Metwaly [a,b,*], Moustafa M. Saleh [c,**], Bshra A. Alsfouk [d], Ibrahim M. Ibrahim [e], Muhamad Abd-Elraouf [a], Eslam B. Elkaeed [f], Ibrahim H. Eissa [g,***]

[a] *Pharmacognosy and Medicinal Plants Department, Faculty of Pharmacy (Boys), Al-Azhar University, Cairo, 11884, Egypt*
[b] *Biopharmaceutical Products Research Department, Genetic Engineering and Biotechnology Research Institute, City of Scientific Research and Technological Applications (SRTA-City), Alexandria, Egypt*
[c] *Microbiology and Immunology Department, Faculty of Pharmacy, Port Said University, Port Said, Egypt*
[d] *Department of Pharmaceutical Sciences, College of Pharmacy, Princess Nourah bint Abdulrahman University, P.O. Box 84428, Riyadh, 11671, Saudi Arabia*
[e] *Biophysics Department, Faculty of Science, Cairo University. Giza 12613, Egypt*
[f] *Department of Pharmaceutical Sciences, College of Pharmacy, AlMaarefa University, Riyadh, 13713, Saudi Arabia*
[g] *Pharmaceutical Medicinal Chemistry & Drug Design Department, Faculty of Pharmacy (Boys), Al-Azhar University, Cairo, 11884, Egypt*

ARTICLE INFO

Keywords:
Patuletin
Staphylococcus aureus
CrtM
Molecular dynamics simulations
PCAT
Anti-virulence
Biofilm
Staphyloxanthin

ABSTRACT

Staphylococcus aureus is a highly prevalent and aggressive human pathogen causing a wide range of infections. This study aimed to explore the potential of Patuletin, a rare natural flavone, as an anti-virulence agent against *S. aureus*. At a sub-inhibitory concentration (1/4 MIC), Patuletin notably reduced biofilm formation by 27 % and 23 %, and decreased staphyloxanthin production by 53 % and 46 % in *Staphylococcus aureus* isolate SA25923 and clinical isolate SA1, respectively. In order to gain a more comprehensive understanding of the *in vitro* findings, several *in silico* analyses were conducted. Initially, a 3D-flexible alignment study demonstrated a favorable structural similarity between Patuletin and **B70**, the co-crystallized ligand of CrtM, an enzyme that plays a pivotal role in the biosynthesis of staphyloxanthin. Molecular docking highlighted the strong binding of Patuletin to the active site of CrtM, with a high affinity of −20.95 kcal/mol. Subsequent 200 ns molecular dynamics simulations, along with MM-GBSA, ProLIF, PLIP, and PCAT analyses, affirmed the stability of the Patuletin-CrtM complex, revealing no significant changes in CrtM's structure upon binding. Key amino acids crucial for binding were also identified. Collectively, this study showcased the effective inhibition of CrtM activity by Patuletin *in silico* and its attenuation of key virulence factors *in vitro*, including biofilm formation and staphyloxanthin production. These findings hint at Patuletin's potential as a valuable therapeutic agent, especially in combination with antibiotics, to counter antibiotic-resistant *Staphylococcus aureus* infections.

* Corresponding author. Pharmacognosy and Medicinal Plants Department, Faculty of Pharmacy (Boys), Al-Azhar University, Cairo, 11884, Egypt.
** Corresponding author
*** Corresponding author
E-mail addresses: ametwaly@azhar.edu.eg (A.M. Metwaly), mostafa.mohamed@pharm.psu.edu.eg (M.M. Saleh), baalsfouk@pnu.edu.sa (B.A. Alsfouk), ibrahim_mohamed@cu.edu.eg (I.M. Ibrahim), mhmraouf@azhar.edu.eg (M. Abd-Elraouf), ekaeed@um.edu.sa (E.B. Elkaeed), ibrahimeissa@azhar.edu.eg (I.H. Eissa).

https://doi.org/10.1016/j.heliyon.2024.e24075
Received 8 October 2023; Received in revised form 18 December 2023; Accepted 3 January 2024
Available online 6 January 2024

1. Introduction

Staphylococcus aureus (*S. aureus*) stands out as one of the most prevalent and aggressive human pathogens [1]. Clinical presentations associated with *S. aureus* infections encompass a wide spectrum, ranging from the respiratory tract and skin infections to severe conditions such as toxic shock syndrome, sepsis, osteomyelitis, meningo-encephalitis, and bacterial endocarditis [2]. Responding to diverse environmental signals, this system enables *S. aureus* to tune the production of critical virulence factors, which are indispensable for its survival within the host as well as for its pathogenicity [3]. These factors encompass cell surface adhesins, extracellular enzymes, and toxins, all of which contribute significantly to the bacterium's pathogenicity and its capacity to evade host defenses [4]. Staphyloxanthin, a distinctive golden pigment produced by *S. aureus*, is a significant contributor to its virulence offering several advantages to the bacterium, including protection against the host's immune defense and increased resistance to oxidative stress [5]. It acts as a potent antioxidant, aiding the *S. aureus* in surviving within the host's immune system. Furthermore, the golden hue produced by staphyloxanthin is responsible for the characteristic appearance of *S. aureus* colonies [6]. Dehydrosqualene synthase, CrtM, is an enzyme that plays a crucial role in the synthesis of staphyloxanthin through facilitating the formation of dehydrosqualene, which serves as a crucial intermediate in the biosynthesis pathway of staphyloxanthin [7]. Dehydrosqualene then undergoes further conversions through a series of enzymatic reactions, ultimately resulting in the production of the final pigment, staphyloxanthin [8].

Understanding the biosynthesis of staphyloxanthin and the roles played by enzymes like CrtM is vital in studying the virulence and pathogenic properties of *S. aureus*. Moreover, this knowledge may potentially lead to the development of innovative strategies for combating staphylococcal infections [9].

The computational drug discovery relies on the application of *in silico* methods, algorithms, and modelling to aid in the quest for new drugs or the repurposing of existing ones [10]. This field leverages software and simulations to scrutinize the interactions between small molecules (ligands), which have the potential to become drug candidates and specific target biomolecules like proteins. The incorporation of computational drug discovery techniques into the drug development process has gained substantial prominence, playing a pivotal role in the practical implementation of predictive modeling in pharmaceutical research and development [11,12].

Throughout the annals of history, the bounties of nature have consistently served as the wellspring for human essentials, spanning the realms of medicinal remedies, sustenance, and beauty enhancements [13]. Remarkably, from 1981 to 2014, natural products constituted nearly one-third of all newly sanctioned drugs approved by the FDA [14,15]. Numerous flavonoids have demonstrated potent anti-virulence properties, with myricetin, for instance, effectively combating *S. aureus* infection by inhibiting multiple virulence factors, including the suppression of staphyloxanthin production via crtM inhibition [16]. Hesperidin, another flavonoid, exerts its inhibitory prowess by targeting SarA and CrtM, effectively thwarting biofilm formation, virulence, and staphyloxanthin synthesis in methicillin-resistant *S. aureus* [17]. Flavone, too, emerges as a potent antagonist of *S. aureus* virulence, specifically targeting the crtM [18]. Notably, Flavone diminishes the production of key virulence factors, staphyloxanthin, and α-hemolysin, in *S. aureus*, further underscoring its anti-virulence potential [19].

Despite its rarity, scientific investigations have delved into and substantiated Patuletin's anticancer [20,21] as well as antimicrobial potential [22,23].

In this study, the notable structural resemblances between Patuletin and **B70**, the co-crystallized ligand of CrtM, along with previous reports on flavonoid CrtM inhibitorion, served as a compelling foundation for various *in silico* investigations that included the flexible alignment to confirm the structural resemblances in addition to the examination of the binding ability between Patuletin and CrtM through molecular docking and deep, 200 ns, molecular dynamics simulations. Followingly, the *in vitro* capabilities of Patuletin to inhibit the CrtM protein and virulence factors of *S. aureus* were examined.

This study is the first to explore the anti-virulence properties of Patuletin against *S. aureus* through the combination of *in vitro* experiments and *in silico* analyses. The use of sub-inhibitory concentrations of Patuletin reveals significant reductions in key virulence factors. The study not only validates Patuletin's inhibitory effects experimentally but also offers a molecular-level understanding of its binding to a crucial enzyme. The proposal of Patuletin as a potential therapeutic agent, particularly in addressing antibiotic-resistant *S. aureus* infections, adds clinical relevance to its pioneering exploration.

2. Materials and methods

2.1. Active compound (patuletin)

Patuletin was obtained from an earlier isolation from *Tagetes patula* flowers [24].

2.2. Bacterial isolates

The standard strain *S. aureus* ATCC 27853 (SA25923) and one clinical *S. aureus* isolate (SA1) were used in this study. Microbiology and Immunology Department, Faculty of Pharmacy, Suez Canal University generously donated the standard strain, and the clinical isolate was obtained from the stock culture collection of the Microbiology and Immunology Department at Faculty of Pharmacy, Port Said University.

2.3. Minimum inhibitory concentration (MIC) determination of patuletin

The MIC of patuletin against *S. aureus* was determined using the broth micro-dilution method following Clinical and Laboratory Standards Institute (CLSI) procedures. In brief, cultures of the *S. aureus* isolates were diluted with Mueller-Hinton broth to a concentration of 107 CFU/ml, and patuletin solutions were prepared with two-fold serial dilutions. A 100 μl aliquot of bacterial suspensions was mixed with 100 μl of the diluted patuletin solution in microtiter plates. The MIC was defined as the lowest patuletin concentration that inhibited bacterial viability after overnight incubation at 37 °C [25].

2.4. Evaluation of the inhibitory effect of patuletin on virulence factors in S. aureus

2.4.1. Assessment of biofilm inhibition

Biofilm production of patuletin against *S. aureus* was assessed following established protocols. Briefly, *S. aureus* isolates were cultured overnight and suspended in tryptone soya broth (TSB) to achieve a concentration of 10ˆ6 CFU/ml. This bacterial suspension, with and without sub-MIC levels of patuletin, was added to microtiter plate wells (200 μl per well) and incubated at 37 °C for 48 h. After carefully removing TSB to eliminate planktonic cells, plates were air-dried and washed with distilled water. Fixing methanol (99 %, 200 μl) was applied for 20 min, followed by a 15-min application of a 1 % crystal violet solution to stain the biofilm. After washing, crystal violet was dissolved in 33 % glacial acetic acid. A spectrofluorometer (Biotek, USA) was then used to measure the absorbance of the solubilized dye at 570 nm [26].

2.4.2. Assessment of staphyloxanthin inhibition

The impact of patuletin on staphyloxanthin pigment production was assessed using the previously outlined method. *S. aureus* isolates were cultured overnight in 5 ml of TSB until they reached an optical density of 2.0, both in the presence and absence of sub-MIC levels of patuletin. After incubation, bacterial cells were collected by centrifugation at 4000 rpm for 10 min at 4 °C, followed by two washes with distilled water. To extract staphyloxanthin pigment, pellets were suspended in 1.5 ml of 99 % methanol and agitated for 2 h at 55 °C in the dark. This was followed by centrifugation, and the cell-free supernatants were measured at OD450 nm using a spectrofluorometer (Biotek, USA) [27].

2.5. Statistical analysis

Regarding the specific method of significance testing for the analysis of patuletin's impact on *S. aureus* virulence factors, the One-Way Analysis of Variance (ANOVA) was employed using GraphPad Prism 7 software. This statistical test was chosen due to its appropriateness for comparing means among multiple groups, as outlined in the statistical methods section of our manuscript. The significance level (alpha) was set at $P > 0.05$. This choice was made to consider a p-value greater than 0.05 as not statistically significant. We believe that this threshold is appropriate for determining the significance of patuletin's impact on the virulence factors of *S. aureus* in our experimental setup. For each experimental condition, three biological tests, and within each biological test, was performed three technical replicates. This rigorous experimental design aimed to ensure the reliability and reproducibility of our findings. The results were then calculated using the means and standard errors for a clear and concise presentation.

2.6. Flexible alignment

In this protocol, the general-purpose panel was employed with the "Prepare ligand" feature enabled. Ionization settings were adjusted using the "Rule-based" method, selecting carboxylate for acid ionization, and primary, secondary, and tertiary amines for base ionization. Ionization enumeration was set to "one protomer." All options were chosen under the "filter smart" setting. Certain tasks like "Generate tautomers," "generate isomers," "Fix bad valencies," and "parallel processing" were disabled. The "generate coordinates" task was set to 3D mode, and the "duplicate structure" task was set to remove duplicates. After preparation, Discovery studio 4.0 was employed to run a 3D Flexible alignment study for Patuletin and **B70** employing the default parameters [28].

2.7. Docking studies

MOE2014 software was operated molecular docking of Patuletin against CrtM protein (PDB ID: 2ZCS) [29]. In brief, the crystal structure of the CrtM protein with **B70** was processed by removing crystallographic water molecules except H_2O482, H_2O515, and H_2O582 which were reported to form water-mediated hydrogen bonds as seen in the reported binding mode of the co-crystallized ligand [30]. One chain, alongside the co-crystallized ligand, was retained. The selected CrtM protein chain underwent protonation using specific settings: GB/VI electrostatic functional form with a 15 Å distance cut-off, dielectric constant set at 2, and a solvent dielectric constant of 80. Van der Waals functional form used was 800R3 with a 10 Å distance cut-off. The protein chain's energy was then minimized using Hamiltonian AM1 in Molecular Operating Environment (MOE 2019) and MMFF94x for structural optimization. The active site for ligand docking (and redocking for validation) was defined as residues within 5 Å distance from **B70**. 2D structures of Patuletin and **B70**, were drawn using ChemBioDraw Ultra 14.0 and saved in MDL-SD file format. Ligand 3D structures were protonated and optimized through energy minimization using MM2 force-field with 10000 iteration steps of 2 fs. The conformationally optimized ligands were utilized for docking studies. The docking configuration for Patuletin and **B70** was arranged based on the established protocol from the validation phase. In each docking run, 30 solutions were generated using ASE for scoring, and a rigid receptor for

refinement. The pose exhibiting the most favorable binding mode was chosen for subsequent analysis. Visualization of the docking outcomes was performed using Discovery Studio 4.0. Evaluation of the docking results involved a comparison of interactions and docking scores between the docked ligand and the reference molecule that was re-docked.

2.8. M D simulations

A 200-ns conventional unbiased molecular dynamics (MD) simulation was performed using GROMACS 2021 to examine the stability of the Protein & Patuletin complex and analyze structural changes between the apo and holo forms of the protein. Input files were created using the CHARMM-GUI server's solution builder module [31,32]. Both the apo protein and the docked complex were placed in a cubic box with dimensions of 8.4 nm. After solvating the system with the TIP3P water model, an additional padding region of 1 nm beyond the furthest atom was included. To achieve system neutrality, NaCl ions were added at a concentration of 0.154 M. The CHARMM36 m force field was used to determine amino acid parameters for the protein, as well as for the TIP3P water model and the neutralizing ions. Patuletin was parameterized using the CHARMM general force field (CGenFF). This part is extensively discussed in the supplementary data section, the procedure is comprehensively delineated and clarified.

2.9. Molecular mechanics/generalized born surface area (MM-GBSA)

The binding energy of the ligand was determined through the application of the MM-GBSA methodology and the gmx_MMPBSA program. Additionally, a decomposition analysis was conducted to discern the specific contributions of individual amino acids situated within a 1-nm radius of the ligand toward the overall binding affinity. To ensure precise calculations, an ionic strength of 0.154 M was utilized along with a selected solvation technique (igb) value of 5. The internal dielectric constant was set at 1.0, while the external dielectric constant was established at 78.5. These settings were chosen to guarantee accuracy and reliability in the obtained results [33] Further extensive discussion is available in the supplementary data section, and the procedure is comprehensively delineated and clarified.

2.10. Protein-ligand interaction fingerprint (ProLIF) study

The interactions between Patuletin and amino acids were assessed and classified in every individual frame utilizing the Protein-Ligand Interaction Fingerprints (ProLIF) Python program. This analysis aimed to identify and evaluate the occurrence and significance of the amino acids involved in stabilizing the Patuletin-CrtM complex. Following this, the trajectory of the protein-ligand complex was subjected to clustering using TTclust. This process allowed for the identification of representative frames from each cluster, aiding in the comprehensive characterization of the complex's behavior over time [34].

2.11. Protein-ligand interaction profile (PLIP) study

The Patuletin-CrtM complex trajectory underwent clustering through TTclust to extract representative frames from various clusters. These selected frames were then subjected to analysis using the Protein-Ligand Interaction Profiler (PLIP) tool. PLIP provided a detailed breakdown of the types and frequencies of interactions present within the frames obtained from the Patuletin-CrtM complex. The output data was formatted in three dimensions and saved as a.pse file, facilitating visualization through PyMol. This allowed for a comprehensive understanding of the intricate interactions between Patuletin and CrtM at a molecular level [35,36].

2.12. Principal component analysis of trajectories (PCAT)

PCAT is employed in this study to assess the mobility of alpha carbons in the amino acids Met6:Tyr284, excluding the N-terminal amino acids. This involves analyzing the mass-weighted covariance matrix (C) of the specified subset of atoms within molecular dynamics (MD) trajectories. Each trajectory's last frame during the equilibrium stage serves as the alignment reference. In combined trajectories, the final frame of the equilibrated apo system is used as the reference structure [37]. PCA, achieved through the diagonalization of the covariance matrix (C), identifies eigenvectors that effectively represent atomic motions. The eigenvalues associated with each principal component (PC) indicate the extent of motion. The highest eigenvalue corresponds to the first principal component, followed by decreasing values indicating reduced motion. Diagonalization is performed using the "gmx covar" program in GROMACS, and subsequent analysis is conducted with "gmx anaeig."

Determining the essential subspace size involves several steps: Calculating the cumulative sum of eigenvalues in ascending order of corresponding eigenvectors. Analyzing the scree plot to pinpoint the point where the slope of the eigenvalue curve experiences the most significant reduction. Considering eigenvector distribution, recognizing that non-random eigenvectors deviate from a Gaussian distribution [38] as extensively discussed in the supplementary data section, the procedure is comprehensively delineated and clarified.

3. Results and discussions

In the context of this research study, the remarkable structural similarities observed between Patuletin and **B70**, which is the co-crystallized ligand of the CrtM protein, coupled with prior research findings on flavonoid compounds as potential inhibitors of CrtM,

formed a compelling basis for our exploration. This prompted us to investigate both the *in vitro* and *in silico* potential of Patuletin against the virulence factors associated with *S. aureus*.

3.1. In vitro studies

3.1.1. Determination of patuletin MIC

The MIC of patuletin was found to be 2 mg/ml by the broth micro-dilution method. Patuletin was further tested for additional anti-virulence effects against *S. aureus* virulence factors at a sub-MIC concentration equivalent to ¼ MIC (0.5 mg/ml) in order to rule out any possible inhibitory activity of the tested substance due to the potential lethal activity on bacterial viability. The identification of an MIC value of 2 mg/ml confirms Patuletin's ability to effectively hinder bacterial growth. This significant discovery provides a basis for delving into the compound's broader influence on virulence factors, extending beyond its direct antimicrobial effects. Employing a sub-inhibitory concentration at 1/4 MIC in subsequent assessments was a thoughtful choice, allowing for the exploration of anti-virulence effects while avoiding potential growth inhibition. This concentration consistently exhibited notable effects on all assessed virulence factors, affirming its appropriateness for further research.

3.2. The inhibitory effect of sub-MIC of patuletin on virulence factors in S. aureus

3.2.1. Biofilm inhibition assessment

The crystal violet method [26] was employed in this study to evaluate the inhibitory impact on biofilm development. It's interesting to note that patuletin significantly decreased biofilm formation ability by a percentage of 27 % and 23 % in SA25923 and SA1-treated isolates in comparison to control untreated isolates, respectively (Fig. 1 A). This inhibition was determined through measuring the absorbance of the solubilized dye, crystal violet (Fig. 1 B), by spectrofluorometer at 570 nm. A noteworthy finding in this study is the substantial decrease in biofilm formation triggered by Patuletin. Biofilm formation plays a crucial role in the virulence of *S. aureus*, as it enhances the organism's ability to withstand and resist conventional antibiotics. The significant reduction observed in SA25923 and SA1-treated isolates suggests the potential of Patuletin as a powerful anti-virulence agent in addressing infections associated with *S. aureus*.

3.2.2. Assessment of staphyloxanthin inhibition

The effect of patuletin on preventing *S. aureus* from producing staphyloxanthin pigment was measured spectrophotometrically. Notably, patuletin significantly decreased staphyloxanthin production by a percentage of 53 % and 46 % in SA25923 and SA1-treated isolates compared with control untreated isolates, respectively (Fig. 2). The noteworthy reduction in staphyloxanthin production, a virulence factor known for its role in evading host defenses, emphasizes the potential therapeutic value of Patuletin. The decrease observed in SA25923 and SA1-treated isolates further highlights the compound's ability to alleviate the detrimental effects associated with this virulence factor. This suggests a promising role for patuletin in combating infections related to staphylococcal pathogens.

3.3. In silico studies

To acquire a more thorough and detailed comprehension of the *in vitro* findings at the molecular level, a series of *in silico* analyses were undertaken. These computational analyses were instrumental in dissecting the intricacies of the experimental results, providing valuable insights into the molecular mechanisms underlying the observed anti-virulence activities of Patuletin.

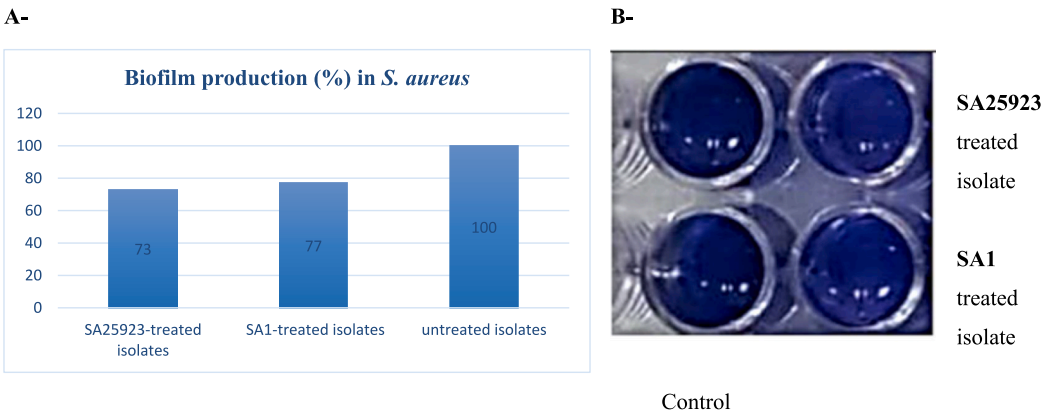

Fig. 1. A. Patuletin reducing potential at 1/4 MIC on *S. aureus* capacity to form biofilms in treated bacteria. Optical density was measured at 570 nm. The data shown represent the means ± standard errors. *P < 0.05.

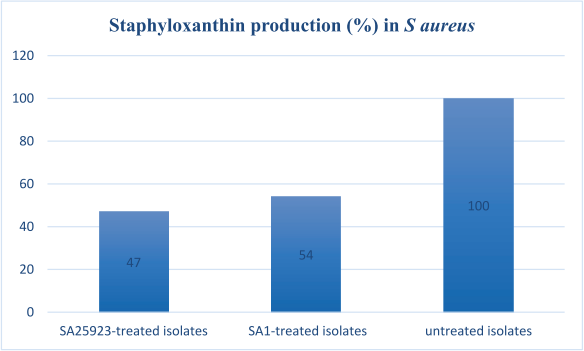

Fig. 2. Patuletin at 1/4 MIC significantly reduced the biosynthesis of staphyloxanthin in *S. aureus* in treated isolates compared to control untreated isolates. Optical density was measured at 450 nm. The data shown represent the means ± standard errors. *P < 0.05.

3.3.1. Flexible alignment

A 3D-Flexible alignment of patuletin with **B70** was carried out. The result (Fig. 3) revealed the general good overlapping. Interestingly, patuletin showed the same spatial orientation as **B70**. In detail, the pyrocatechol moiety of patuletin showed the same orientation as the terminal phenyl moiety of B70. Additionally, 3-Hydroxy-4H-pyran-4-one moiety of patuletin exhibited close orientation to the central phenyl ring of **B70**. Furthermore, 2-methoxybenzene-1,3-diol moiety of patuletin showed the same orientation as the 1-phosphonopentane-1-sulfonic acid moiety of B70.

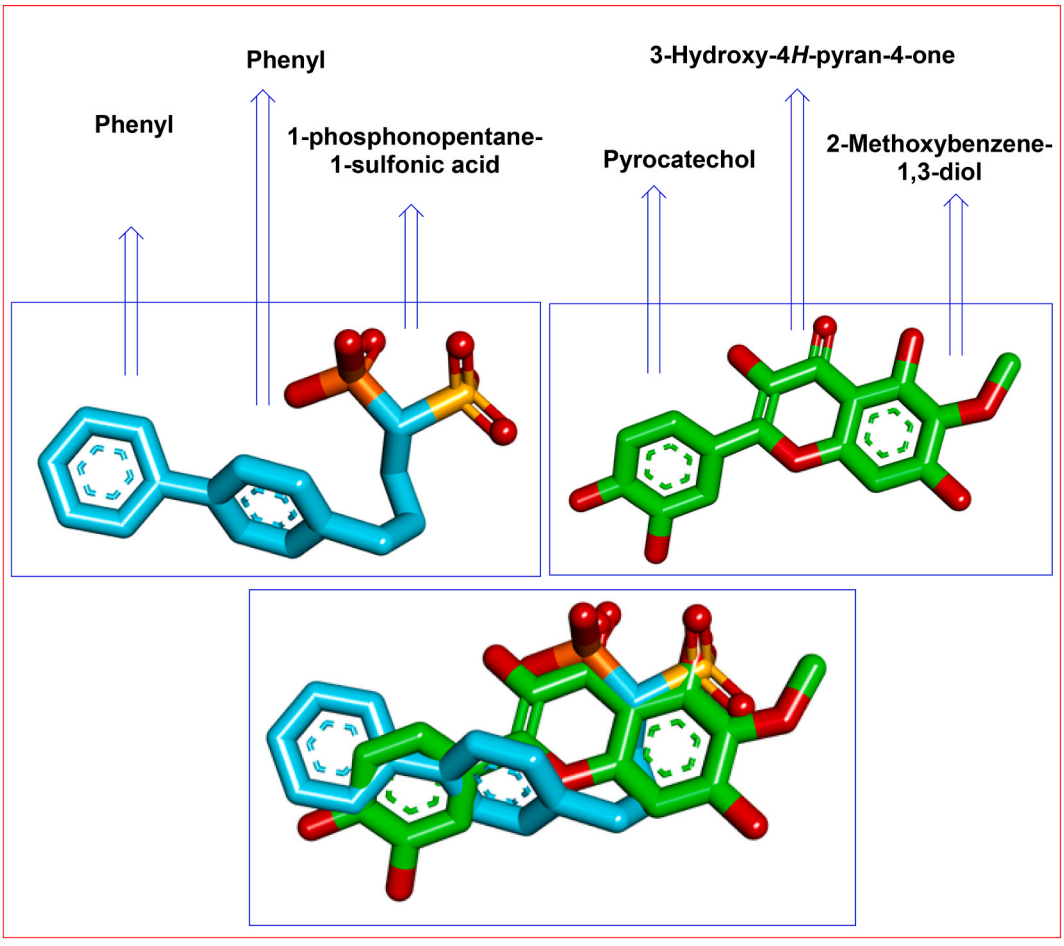

Fig. 3. Flexible alignment of patuletin (dark green) with B70 (turquoise).

3.3.2. Molecular docking

The substantial structural similarities between Patuletin and **B70**, the co-crystallized ligand of the CrtM protein, have sparked considerable interest in exploring Patuletin's potential as an inhibitor of CrtM. This structural resemblance suggests that Patuletin might interact with the CrtM protein in a manner akin to **B70**, opening up the possibility of similar inhibitory effects. Furthermore, the context of previously reported flavonoid inhibitors adds weight to this investigation, as it suggests that Patuletin, as a member of the flavonoid family, might possess inhibitory properties against CrtM similar to those observed in related compounds. To comprehensively explore Patuletin's interactions with the CrtM protein, we started with a molecular docking technique against the dehydrosqualene synthase (CrtM) (PDB ID: 2ZCS) which was retrieved from the Protein Data Bank. The co-crystallized ligand of such protein, tripotassium (1R)-4-biphenyl-4-yl-1-phosphonatobutane-1-sulfonate (**B70**), was used as a reference molecule.

At first, validation of the docking process was tested through running the docking procedure for only the co-crystallized ligand against the active site. It was found that the produced RMSD value between the generated pose of the docked molecule and the original one equal 0.93 Å. This indicates the validity of the docking process (Fig. 4).

Regarding the binding mode of the co-crystallized ligand of CrtM (**B70**) against CrtM, it exhibited a binding score of −20.80 kcal/mol. The phenyl tail was oriented into the first pocket of the active site forming three hydrophobic interactions with Leu160, Ala157, and Leu141. The central phenyl ring occupied the central region of the active site forming three hydrophobic interactions with Ala134, Leu164, and Val137. In addition, it formed an electrostatic interaction with Phe22. The hydrophilic head of the co-crystallized ligand (1-phosphonopentane-1-sulfonic acid) was buried in the third pocket of the active site forming eight hydrogen bonds with Gln165, Arg171, Ser19, Tyr248, Arg45, His18, Tyr41, and H_2O482. In addition, three electrostatic bonds were formed between the hydrophilic head and Phe22, Tyr41, and Tyr248. The detailed 3D, 2D and mapping surface of the **B70**'s binding mode were presented in Fig. 5A and 5B, and Fig. 5C, respectively.

Patuletin showed an acceptable binding mode against CrtM with binding energy of −16.87 kcal/mol it occupied the active site of CrtM. The pyrocatechol moiety occupied the first pocket of the active site to form three hydrophobic interactions with Leu164, Val137, and Ala134. In addition, it formed an electrostatic attraction with Phe22. Furthermore, the 3-hydroxy-4H-pyran-4-one moiety formed one hydrophobic interaction with Ala134. Furthermore, the 2-methoxybenzene-1,3-diol moiety was buried in the third pocket of the active site forming five hydrogen bonds with Arg45, His18, Ser19, and H_2O482 The detailed 3D, 2D and mapping surface of the Patuletin's binding mode were presented in Fig. 6 A, Fig. 6 B, and Fig. 6C, respectively.

3.3.3. MD simulations

Molecular dynamics (MD) simulations emerge as a potent tool to provide substantial insights into the dynamic alterations, adaptability, and interplays of biomolecules, encompassing proteins (receptors) and nucleic acids. These simulations exhibit wide-ranging utility across various domains of research, spanning structural biology, biochemistry, drug exploration, and materials science. The knowledge gleaned from MD simulations acts in synergy with empirical data, facilitating a comprehensive grasp of the intricate mechanisms governing molecular processes, interactions between proteins and ligands, the intricate choreography of protein folding, and numerous other pivotal biological occurrences [39]. A 200 ns production run was applied. Interestingly, the stability of both the distance between Patuletin and the CrtM's center of mass and the structural integrity of the CrtM remained stable. Fig. 7A depicts the root-mean-square deviation (RMSD) values of the apo CrtM (blue line), which reached a stable state around 1.7 Å. In contrast, the holo CrtM (red line) exhibited two slightly distinct states. During the initial 100 ns, it maintained an average value of approximately 1.7 Å, which then slightly increased to around 2 Å in the latter half. The RMSD value for Patuletin remained relatively consistent at an average of 4 Å, indicating the presence of a stable conformation (Fig. 7B), albeit different from the initial configuration. Fig. 7.C and 7.D presents data indicating that the apo system and holo system displayed similar average values for the radius of gyration (RoG) and solvent accessible surface area (SASA), respectively. Fig. 7E illustrates the average number of hydrogen bonds formed between Patuletin and CrtM. The data reveals a consistent formation of at least one hydrogen bond between Patuletin and CrtM, with a maximum of three hydrogen bonds, suggesting a sustained interaction between the two components. In summary, the findings demonstrate stability in both the apo and holo CrtMs, with no significant structural alterations observed in either system. Additionally, a slight difference is evident in the oscillatory behavior of C-alpha atoms when comparing the root-mean-square fluctuations (RMSFs)

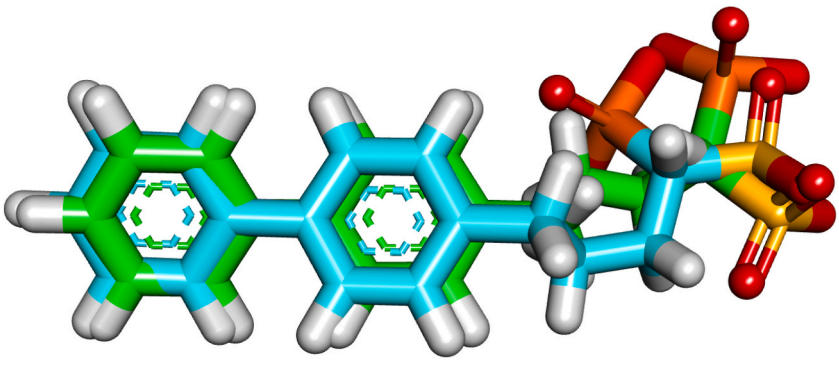

Fig. 4. Superimposition of the co-crystallized molecule (turquoise) and the docking pose (dark green) of the same molecule.

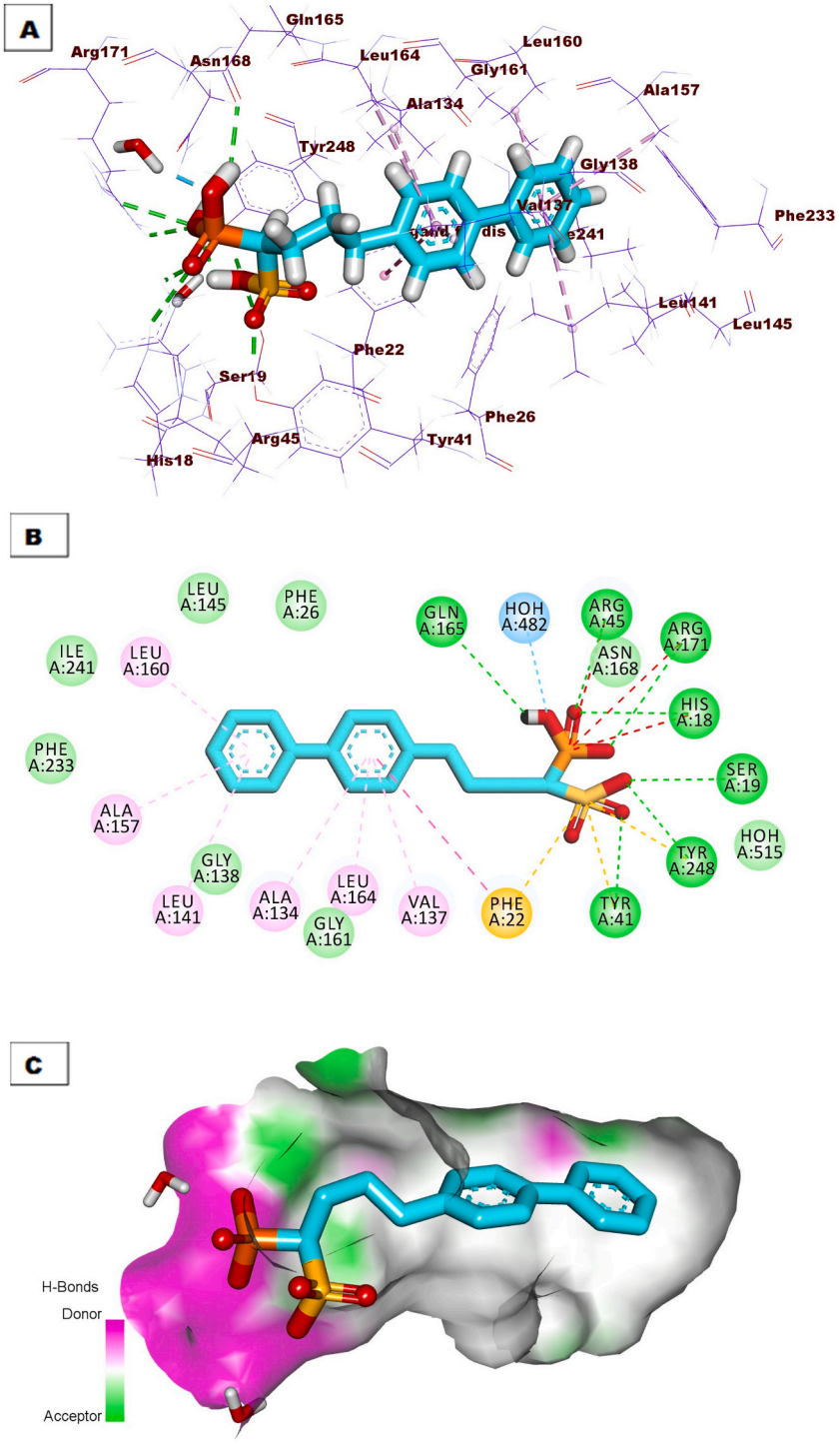

Fig. 5. A) 3D interaction of B70 against the active site of CrtM. B) 2D interaction of B70 in the active site of CrtM. C) Mapping surface showing B70 occupying the active pocket of CrtM.

of the two systems. Notably, the holo system exhibits slightly larger fluctuations in the Glu76:His78 loop, while the remaining regions of the two CrtMs exhibit similar RMSF values and less than 2 Å, except for the N-terminal (Fig. 7F). Patuletin consistently maintains an average distance of approximately 3.3 Å between the centers of mass of the CrtM and the ligand, indicating a stable binding (Fig. 7G).

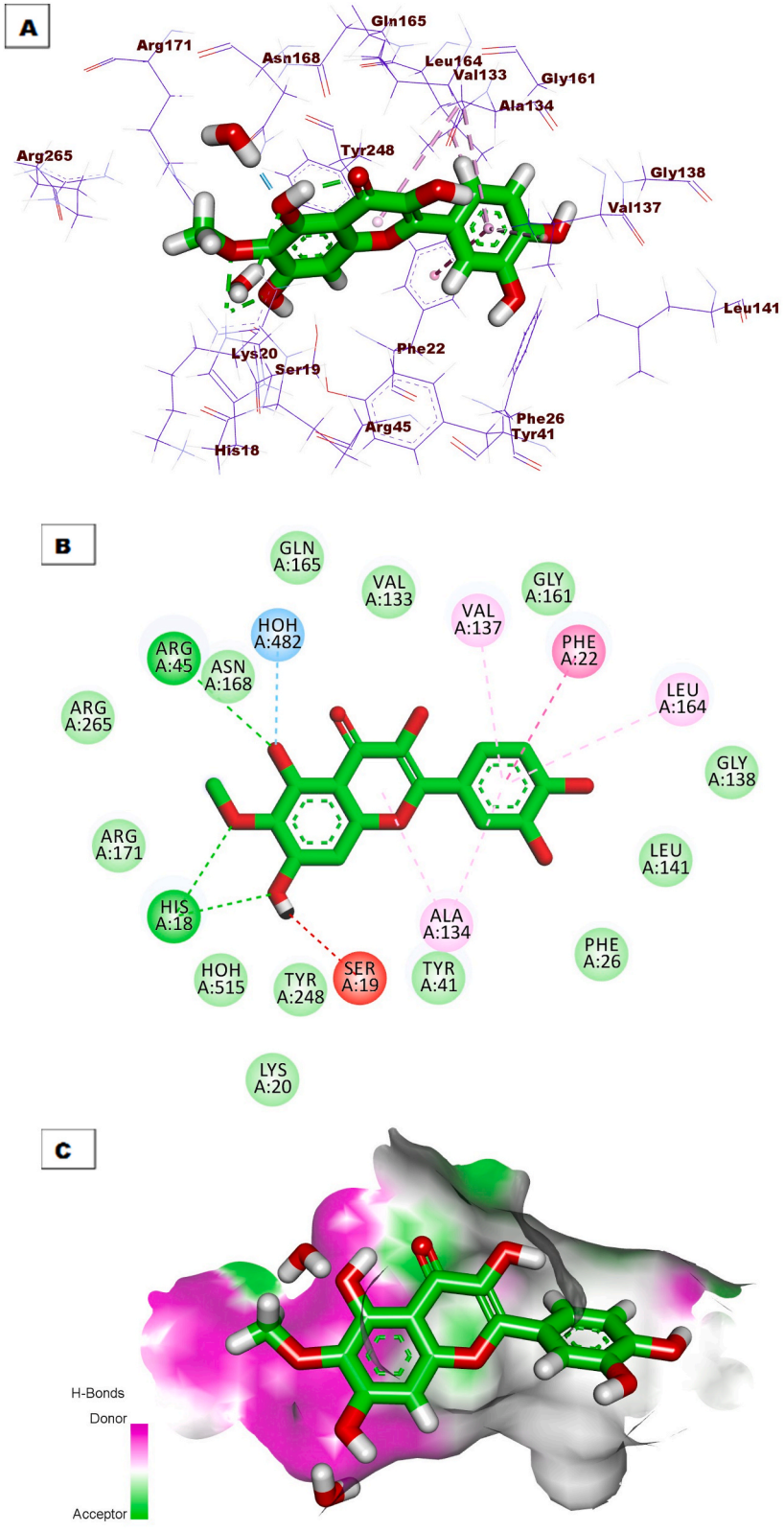

Fig. 6. A) 3D interaction of patuletin in the active site of CrtM. B) 2D interaction of Patuletin in the active site of CrtM. C) Mapping surface showing patuletin occupying the active pocket of CrtM.

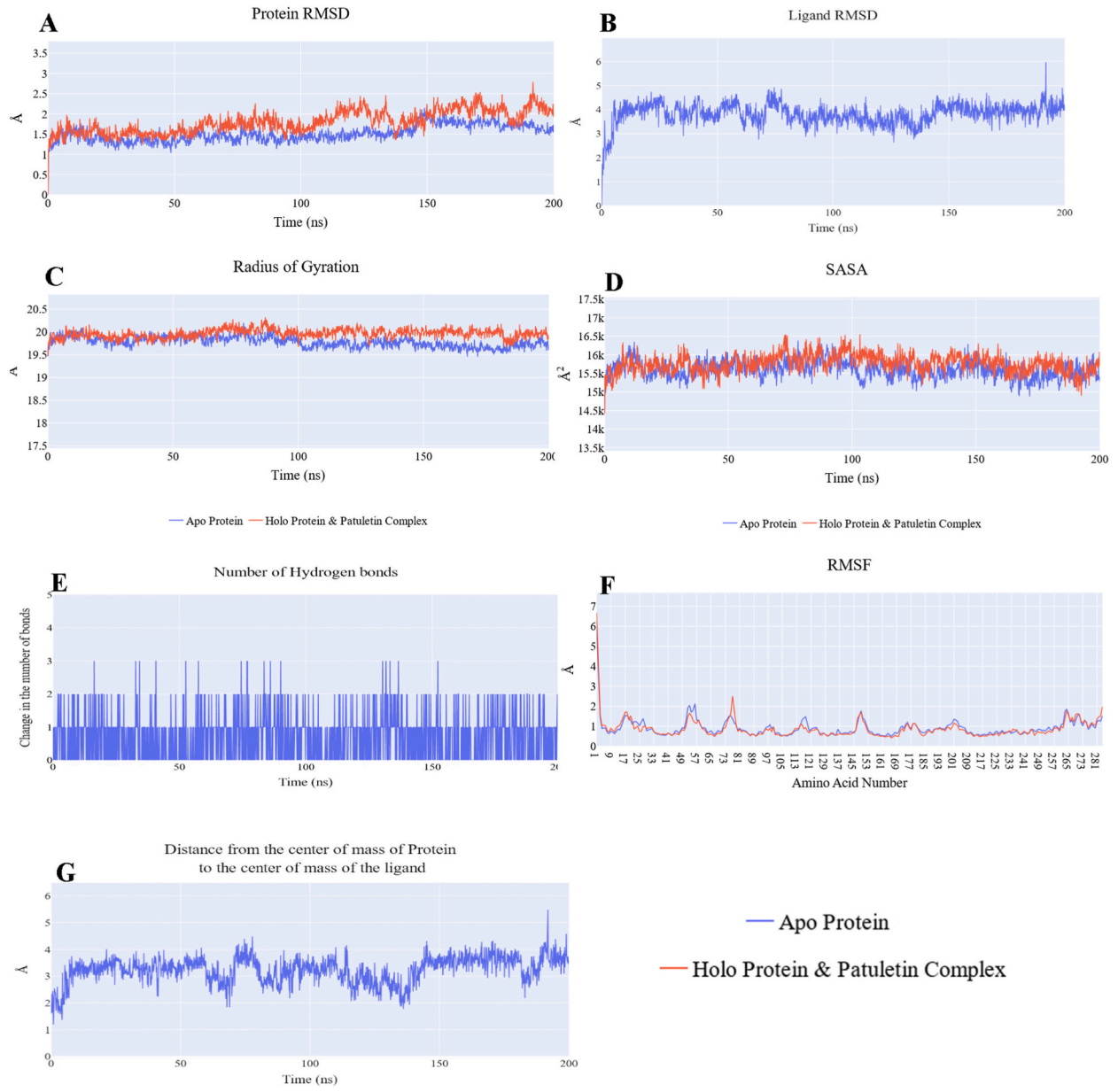

Fig. 7. A) RMSD graph of CrtM, B) Patuletin's RMSD graph, C) RoG for the CrtM, D) SASA for the CrtM, E) hydrogen bond alternation between CrtM and Patuletin, F) RMSF graph for the CrtM, G) distance from the center of mass of Patuletin and CrtM.

3.3.4. MM-GBSA studies

Fig. 8 presents a comprehensive depiction of the computed components comprising the estimated binding free energy using the MM-GBSA methodology. The considerable interaction between Patuletin and the CrtM can be inferred from its average binding energy value of −30.76 kcal/mol. Notably, the evaluation of binding stability highlights the prominent role of Van der Waals contacts, which contribute significantly with energy of −40.79 kcal/mol, surpassing the energetics of electrostatic interactions at −24.17 kcal/mol. To further elucidate the specific amino acids involved, decomposition analysis was performed, focusing on those within a proximity of 1 nm from Patuletin, as illustrated in Fig. 9. The analysis revealed individual contributions from various amino acids, with Phe22 (−3.98 kcal/mol), Tyr41 (−2.12 kcal/mol), Ala134 (−2.59 kcal/mol), Val137 (−1.65 kcal/mol), Ala157 (−1.04 kcal/mol), Leu160 (−1.15 kcal/mol), and Leu164 (−1.68 kcal/mol) exhibiting contributions of less than −1 kcal/mol.

3.3.5. Protein-ligand interaction fingerprint (ProLIF) study

ProLIF, an acronym for Protein-Ligand Interaction Fingerprinting, stands as a crucial technique within the realm of computer-aided drug design and molecular docking investigations. This method entails the generation of interaction fingerprints, essentially digital

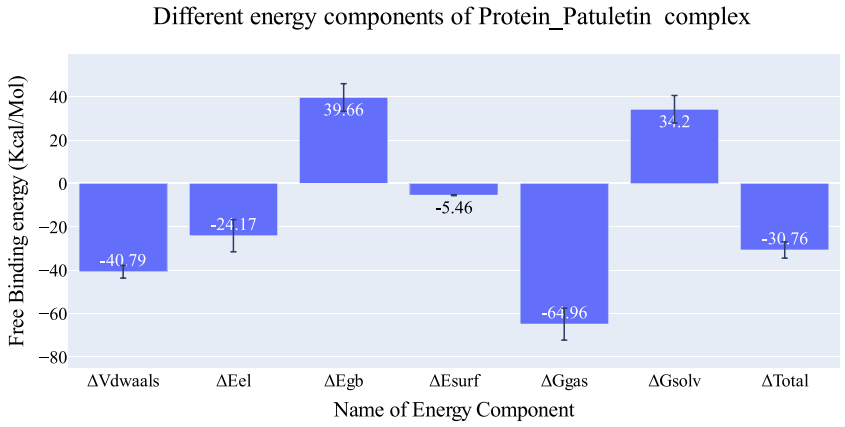

Fig. 8. MM-GBSA components of energies of the CrtM_Patuletin complex. Bars represent the standard deviations.

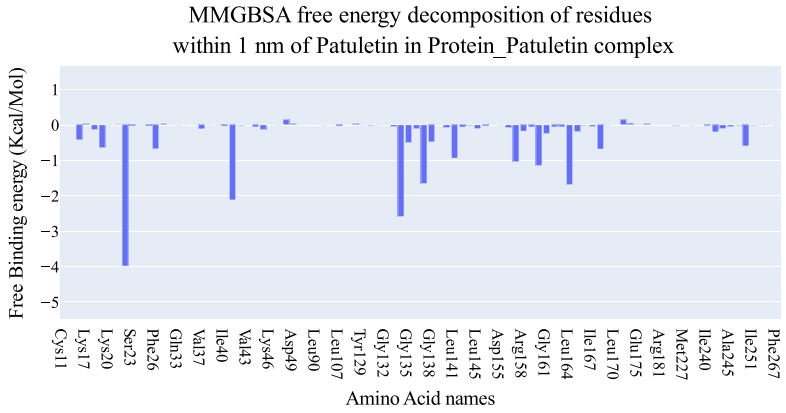

Fig. 9. The analysis of the CrtM_Patuletin complex binding free energy.

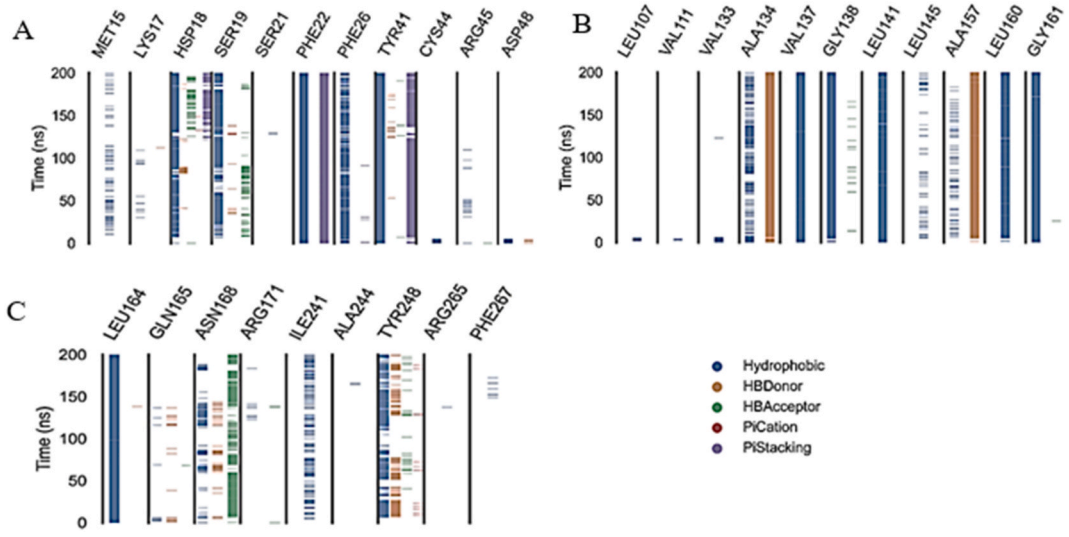

Fig. 10. The amino acids involved, the types of interactions they engaged in the CrtM_Patuletin complex employing the ProLIF Python library. The amino acids were presented in three groups (A, B and C).

footprints, that vividly depict the intricate interplay between a protein and a ligand. These fingerprints serve as a means to meticulously scrutinize and characterize the binding interactions shared by the protein and ligand. Within the intricate web of MD simulations, ProLIF serves as a powerful tool to dissect the dynamic dynamics of protein-ligand complexes across time. It accomplishes this by illuminating how these interactions evolve during the simulation, thus shedding light on the complex's stability and the strength of their binding affinity. Moreover, ProLIF doesn't merely paint a broad stroke; it provides a fine-grained analysis of diverse interaction types, including hydrogen bonds, hydrophobic contacts, and various non-covalent interactions, enriching our comprehension of these vital molecular partnerships [40]. The analysis conducted using the ProLIF library (Fig. 10) yielded significant insights regarding the hydrophobic binding occurrences of various amino acids that arranged in three groups (Fig. 10A, B and C) for an easier demonstration. Specifically, seven amino acids, namely Phe22 (99.8 %), Tyr41 (98.6 %), Val137 (92.5 %), Glu138 (98 %), Leu141 (83.9 %), Gly161 (94.4 %), and Leu164 (94.8 %), demonstrated a high level of interaction with the molecule (Fig. 10), with binding incidences ranging from 83.9 % to 99.8 %. Additionally, Ala134 and Ala157 were observed to form hydrogen bonds with frequencies of 97.6 % and 89.8 %, respectively. Furthermore, Phe22 exhibited a Pi-stacking interaction with an occurrence of 95.3 %.

3.3.6. PLIP study

PLIP, a bioinformatics tool of great importance, serves as a critical component in the analysis and visualization of interactions occurring within molecular complexes involving proteins and ligands. Its primary function is to provide invaluable insights into the binding interactions and non-covalent contacts that take place between the ligand and the protein. This information is pivotal in unraveling the intricate molecular mechanisms underlying these ligand-receptor interactions. PLIP's significance extends across various domains, including drug discovery, computational biology, and structural bioinformatics. PLIP widely employed to thoroughly investigate protein-ligand complexes and the interactions they entail. When combined with other computational techniques like molecular docking, molecular dynamics (MD) simulations, and free energy calculations, PLIP offers a comprehensive understanding of the complex interplay between ligands and proteins. Consequently, it stands as an indispensable tool in the realm of rational drug design, facilitating the development of novel therapeutic agents [41]. To visualize the three-dimensional binding interactions, representative frames were extracted as.pse files using PLIP (). The PLIP of the CrtM_Patuletin complex revealed the identification of four distinct clusters denoted as C1, C2, C3, and C4, as illustrated in Fig. 11. Each cluster was characterized by a comprehensive depiction of hydrophobic interactions and hydrogen bonds in the three-dimensional space. Fig. 11 provides a detailed visualization of

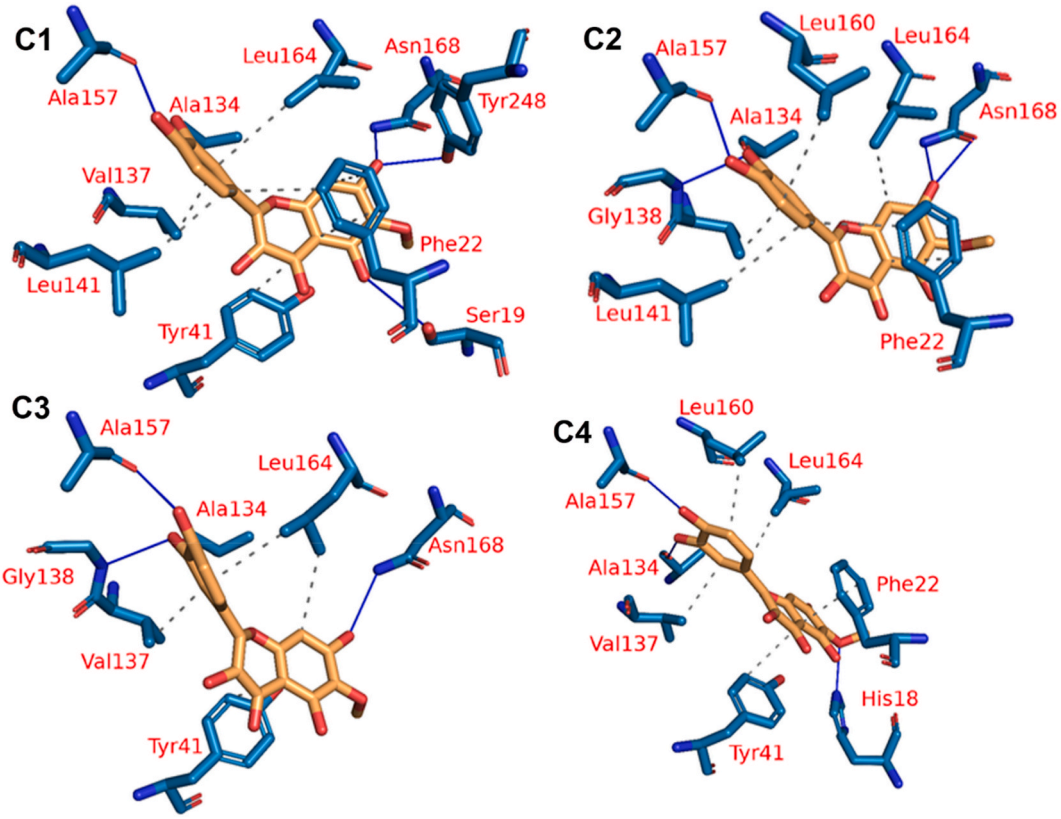

Fig. 11. Representation of the obtained four clusters in the CrtM_Patuletin complex from the TTClust and their 3D interactions. Four distinct clusters were obtained and denoted as C1, C2, C3, and C4. Grey dashed lines: hydrophobic interactions, blue solid lines: H-bonds, orange sticks: Patuletin, blue sticks: CrtM's amino acids.

the molecular interactions within each cluster, highlighting the spatial arrangement of hydrophobic contacts and the specific hydrogen bonding patterns.

By comparing the binding energies obtained from the MM-GBSA approach with the ProLIF results, it becomes apparent that Phe22, Tyr41, Ala134, Val137, Ala157, and Leu164 are consistently identified, suggesting that these amino acids may serve as hot spots for the interaction.

3.3.7. Principal component analysis of trajectories (PCAT) analysis

PCAT, a commonly employed computational technique in MD simulations, serves a pivotal role in the analysis of critical collective motions extracted from trajectory data. During an MD simulation, the positions of atoms within a biomolecular system are meticulously recorded over time, resulting in a comprehensive trajectory that captures the dynamic nature of the system. PCAT steps in to simplify this complexity by projecting the trajectory into a lower-dimensional space while retaining the most significant motions. By distilling the trajectory, PCAT enables to zero in the predominant movements that dictate the behavior and function of the biomolecular system. This, in turn, provides invaluable insights into the fundamental collective motions governing the system, thereby aiding in the identification of synchronized movements [42]. PCAT was employed to elucidate the coordinated motions within the dataset. The determination of the appropriate dimensionality for the reduced subspace was conducted utilizing various metrics, as explained in detail in the methods section. Notably, the scree plot exhibited a distinct change in slope at the second principal component (PC). The first eigenvector captured approximately 73.5 % of the total variance, while the cumulative contribution of the first three eigenvectors accounted for approximately 81.1 % of the overall variation (Fig. 12). Furthermore, the distribution of the first three PCs deviated from a Gaussian distribution, as evident in Fig. 13. Consequently, based on these findings, we selected the first three eigenvectors as the representative reduced subspace for the fundamental subspace.

3.3.8. Cosine content study

To assess the level of randomness observed in the behavior of the initial ten eigenvectors, the cosine content was computed for both the apo and holo CrtM simulations. The analysis revealed that the cosine content of the first ten eigenvectors was below 0.2 for both systems (Fig. 14). Furthermore, the Root Mean Square Inner Product (RMSIP) analysis demonstrated a substantial overlap between the two subspaces, specifically the first three eigenvectors, with a value of 33.2 %. Moreover, the RMSIP analysis indicated a similarity of 44 % between the C matrices of the apo and holo CrtMs, suggesting a comparable sampling in the two systems.

The results obtained from projecting individual trajectories onto the first three eigenvectors of the newly derived C matrix are presented in Fig. 15. Each graph includes a larger dot representing the average structure of the respective trajectory. Fig. 15. A focuses on the projection onto the first two eigenvectors, revealing distinct average structures between the two trajectories. Additionally, the frames demonstrate separate sampling, with only a limited degree of overlap observed at the initial stages of the simulation, as indicated by pale red and white dots. Moving on to Fig. 15. B, which illustrates the projection onto PC1 and PC3, it becomes apparent that there is an initial overlap between the two trajectories, yet they exhibit different average structures. Finally, Fig. 15. C displays the projection onto the second and third eigenvectors, demonstrating a similar projection pattern. In addition, the two trajectories exhibit clustering behavior with a small degree of overlap during the early stages of the simulation.

This research provides strong support for the ability of patuletin to combat the virulence of *S. aureus*. It emerges as a promising candidate for further development as a complementary therapy, adding a fresh approach to the fight against staph infections. Prior studies have highlighted the potential of compounds like myricetin [43], hesperetin [44], naringenin [45], and phloretin [46] in exhibiting promising anti-virulence effects against *S. aureus*. This collective body of evidence underscores the potential of flavonoids as a class of compounds with significant anti-virulence properties, warranting continued investigation for their therapeutic potential.

This research presented for the first time both *in vitro* experiments and *in silico* analyses to thoroughly investigate the anti-virulence properties of Patuletin against *S. aureus*. The use of sub-inhibitory concentrations of Patuletin in the experiments is a notable point, as it reveals significant effects on key virulence factors, providing insights that could be crucial for potential therapeutic applications. The inclusion of molecular analyses, such as 3D-flexible alignment, molecular docking, and molecular dynamics simulations for long time (200 ns), contributes to the precision of the study, offering a detailed understanding, on a molecular levels, of how Patuletin interacts with CrtM, a crucial enzyme in *S. aureus*.

The utilization of *in silico* methods for toxicity prediction has become a crucial asset in drug development. This approach plays a pivotal role in circumventing ethical regulations, addressing limitations in resources, and averting the time-consuming nature of traditional *in vitro* and *in vivo* studies [47] Interestingly, the comparative analysis between Patuletin and Remdesivir was presented before [24]. Patuletin was predicted as non-mutagenic in the Ames test, contrasting with Remdesivir's mutagenic prediction. In terms of carcinogenic potency, Patuletin exhibits a higher TD_{50} in rats, suggesting potentially lower carcinogenic effects compared to Remdesivir. However, the maximum tolerated dose and oral LD_{50} in rats for Patuletin are notably higher than those for Remdesivir, indicating a much lower acute toxicity. Furthermore, Patuletin demonstrates a substantially higher chronic LOAEL in rats, implying very low sensitivity to adverse effects with prolonged exposure. These findings have crucial implications for the safety assessment and potential therapeutic use of Patuletin.

However, it's important to acknowledge certain limitations, including a broader range of isolates could strengthen the study's applicability to diverse strains. Additionally, while these initial findings are encouraging, it is essential to conduct further studies to validate the clinical potential of patuletin. This includes carrying out *in vivo* experiments which will provide crucial information regarding its practical application in clinical settings. Also, gaining a deeper understanding of the specific molecular mechanisms responsible for Patuletin's anti-virulence effects will offer valuable insights into its mode of action. Given that dehydrosqualene synthase has been identified as the proposed biological target, it will be a primary focus in our future plan. This entails rigorous testing

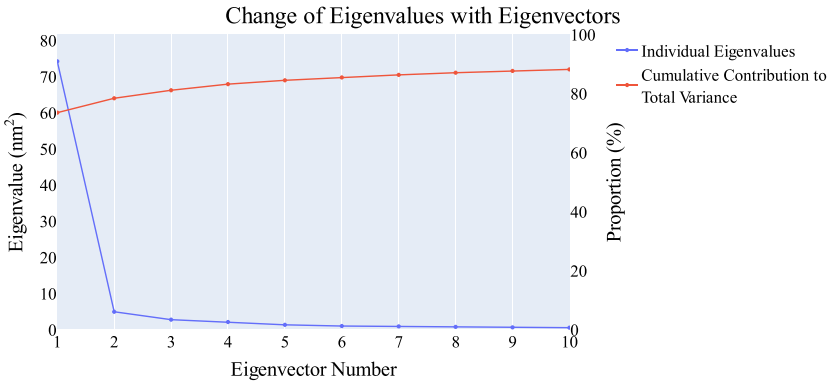

Fig. 12. The eigenvalues alternation.

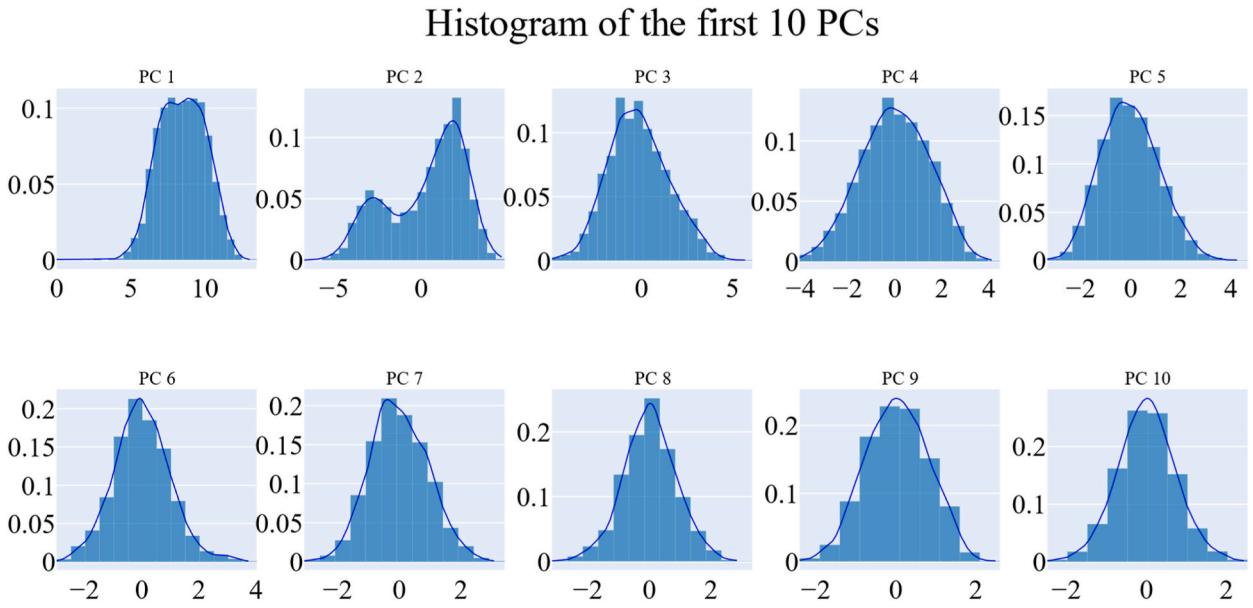

Fig. 13. The distribution of the 1st ten (PC 1-PC 10) eigenvectors.

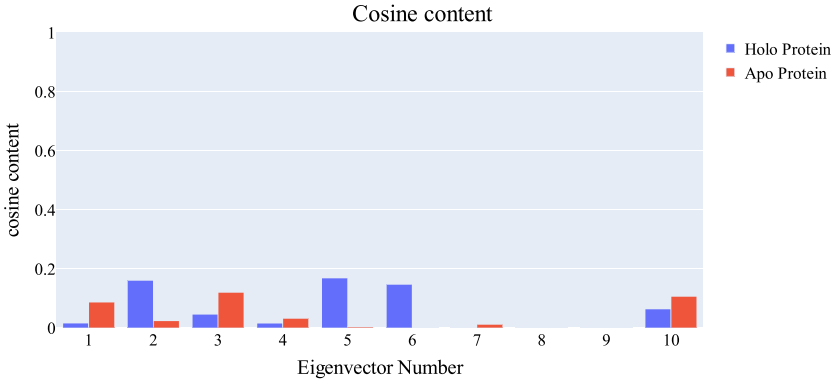

Fig. 14. Shows the values of the cosine content of the first ten eigenvectors for the two trajectories.

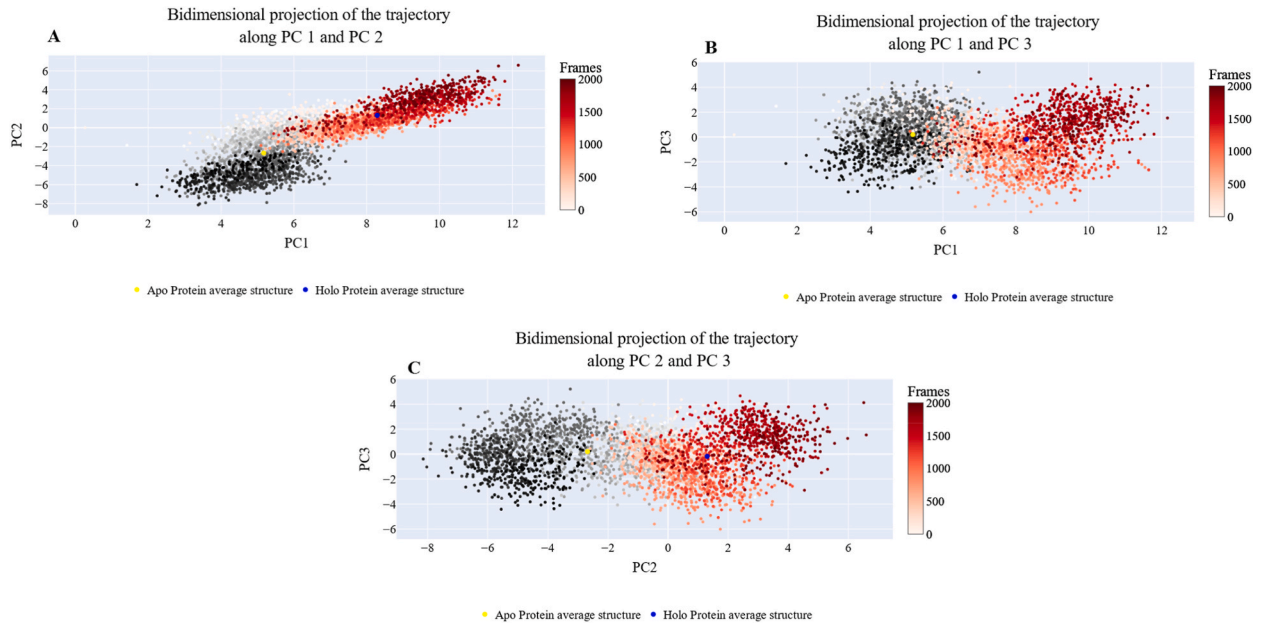

Fig. 15. The projection of each trajectory on A) the 1st 2, B) 1st and 3rd, C) 2nd and 3rd eigenvectors. Small white-to-black dots are the frames of the CrtM in the Apo simulation, small white-to-red dots are the frames of the CrtM in the holo simulation.

to ascertain the efficacy of inhibiting this enzyme as a potential therapeutic strategy. Moreover, an additional pathway of our investigation will involve exploring the synergistic activity of patuletin in combination with FDA-approved antibiotics. This combined approach aims to leverage the potential benefits of patuletin in conjunction with established antibiotics to enhance their effectiveness in combating microbial infections.

4. Conclusion

In conclusion, the comprehensive *in vitro* and *in silico* analyses conducted in this study provide strong evidence for the potential of Patuletin as a promising anti-virulence agent against *S. aureus*. The structural similarity and high binding affinity observed between Patuletin and CrtM, coupled with the stability of the Patuletin-CrtM complex, emphasize its suitability as a CrtM inhibitor. Furthermore, the significant reduction in biofilm formation and staphyloxanthin production in *S. aureus* isolates highlights Patuletin's effectiveness in attenuating key virulence factors. These findings hold significant promise for Patuletin's future application as a therapeutic agent, especially in combination with antibiotics, to combat antibiotic-resistant *S. aureus* infections. Further research and clinical trials are warranted to fully assess the safety and efficacy of Patuletin in practical medical settings.

Data availability statement

All data regarding the presented work was included in the main manuscript and the supplementary materials.

CRediT authorship contribution statement

Ahmed M. Metwaly: Writing - original draft, Project administration, Conceptualization. **Moustafa M. Saleh:** Supervision, Methodology, Investigation. **Bshra A. Alsfouk:** Writing - review & editing, Investigation, Funding acquisition. **Ibrahim M. Ibrahim:** Methodology, Investigation. **Muhamad Abd-Elraouf:** Methodology, Investigation. **Eslam B. Elkaeed:** Writing - review & editing, Investigation. **Ibrahim H. Eissa:** Supervision, Software.

Declaration of competing interest

The authors declare that they have no known competing financial interests or personal relationships that could have appeared to influence the work reported in this paper.

Acknowledgments

This research was funded by Princess Nourah bint Abdulrahman University Researchers Supporting Project number

(PNURSP2024R142), Princess Nourah bint Abdulrahman University, Riyadh, Saudi Arabia. The authors extend their appreciation to the Research Center at AlMaarefa University for funding this work.

Appendix A. Supplementary data

Supplementary data to this article can be found online at https://doi.org/10.1016/j.heliyon.2024.e24075.

References

[1] B.P. Howden, et al., Staphylococcus aureus host interactions and adaptation, Nat. Rev. Microbiol. 21 (6) (2023) 380–395.
[2] F.D. Lowy, Staphylococcus aureus infections, N. Engl. J. Med. 339 (8) (1998) 520–532.
[3] G.Y.C. Cheung, et al., Bacterial virulence plays a crucial role in MRSA sepsis, PLoS Pathog. 17 (2) (2021) e1009369.
[4] G.Y.C. Cheung, J.S. Bae, M. Otto, Pathogenicity and virulence of Staphylococcus aureus, Virulence 12 (1) (2021) 547–569.
[5] L. Xue, et al., Staphyloxanthin: a potential target for antivirulence therapy, Infect. Drug Resist. 12 (2019) 2151–2160.
[6] R.A. Elmesseri, et al., Staphyloxanthin as a potential novel target for deciphering promising anti-Staphylococcus aureus agents, Antibiotics (Basel) 11 (3) (2022).
[7] F.Y. Lin, et al., Mechanism of action and inhibition of dehydrosqualene synthase, Proc. Natl. Acad. Sci. U. S. A. 107 (50) (2010) 21337–21342.
[8] A. Pelz, et al., Structure and biosynthesis of staphyloxanthin from Staphylococcus aureus, J. Biol. Chem. 280 (37) (2005) 32493–32498.
[9] M.E. Cueno, K. Imai, Network analytics approach towards identifying potential antivirulence drug targets within the Staphylococcus aureus staphyloxanthin biosynthetic network, Arch. Biochem. Biophys. 645 (2018) 81–86.
[10] E. Sun, F.E.J.G. Cohen, Computer-assisted drug discovery—a review 137 (1) (1993) 127–132.
[11] A.V. Sadybekov, V. Katritch, Computational approaches streamlining drug discovery, Nature 616 (7958) (2023) 673–685.
[12] S. Brogi, Computational approaches for drug discovery, Molecules 24 (17) (2019).
[13] A.M. Metwaly, et al., Traditional ancient Egyptian medicine: a review, Saudi J. Biol. Sci. 28 (10) (2021) 5823–5832.
[14] A.M. Metwaly, et al., Black ginseng and its saponins: preparation, phytochemistry and pharmacological effects, Molecules 24 (10) (2019) 1856.
[15] D.J. Newman, G.M. Cragg, Natural products as sources of new drugs from 1981 to 2014, J. Nat. Prod. 79 (3) (2016) 629–661.
[16] L.N. Silva, et al., Myricetin protects Galleria mellonella against Staphylococcus aureus infection and inhibits multiple virulence factors, Sci. Rep. 7 (1) (2017) 2823.
[17] K. Vijayakumar, S. Muhilvannan, M. Arun Vignesh, Hesperidin inhibits biofilm formation, virulence and staphyloxanthin synthesis in methicillin resistant Staphylococcus aureus by targeting SarA and CrtM: an in vitro and in silico approach, World J. Microbiol. Biotechnol. 38 (3) (2022) 44.
[18] Z. Tao, et al., Flavone inhibits Staphylococcus aureus virulence via inhibiting the sae two component system, Microb. Pathog. 180 (2023) 106128.
[19] J.H. Lee, et al., Flavone reduces the production of virulence factors, staphyloxanthin and α-hemolysin, in Staphylococcus aureus, Curr. Microbiol. 65 (6) (2012) 726–732.
[20] J.J. Alvarado-Sansininea, et al., Quercetagetin and patuletin: antiproliferative, necrotic and apoptotic activity in tumor cell lines, Molecules 23 (10) (2018).
[21] I.H. Eissa, et al., A new anticancer semisynthetic theobromine derivative targeting EGFR protein: CADDD study, Life 13 (1) (2023) 191.
[22] S. Faizi, et al., Antibacterial and antifungal activities of different parts of Tagetes patula.: Preparation of patuletin derivatives 46 (5) (2008) 309–320.
[23] M.a.L. Tereschuk, et al., Antimicrobial activity of flavonoids from leaves of Tagetes minuta, J. Ethnopharmacol. 56 (3) (1997) 227–232.
[24] A.M. Metwaly, et al., The computational preventive potential of the rare Flavonoid, Patuletin, isolated from Tagetes patula, against SARS-CoV-2, Plants 11 (14) (2022) 1886.
[25] M.P. Weinstein, J.S. Lewis, 2nd, the clinical and laboratory standards Institute subcommittee on antimicrobial susceptibility testing: background, organization, functions, and processes, J. Clin. Microbiol. 58 (3) (2020).
[26] S. Stepanović, et al., Quantification of biofilm in microtiter plates: overview of testing conditions and practical recommendations for assessment of biofilm production by staphylococci, Apmis 115 (8) (2007) 891–899.
[27] M. Kossakowska-Zwierucho, et al., Factors determining Staphylococcus aureus susceptibility to photoantimicrobial chemotherapy: RsbU activity, staphyloxanthin level, and membrane fluidity, Front. Microbiol. 7 (2016) 1141.
[28] E.B. Elkaeed, et al., Computer-assisted drug discovery of potential natural inhibitors of the SARS-CoV-2 RNA-dependent RNA polymerase through a multi-phase in silico approach, Antivir. Ther. 28 (5) (2023) 13596535231199838.
[29] Y.M. Suleimen, et al., Isolation and in silico inhibitory potential against SARS-CoV-2 RNA polymerase of the rare kaempferol 3-O-(6 ″-O-acetyl)-Glucoside from calligonum tetrapterum, Plants 11 (15) (2022) 2072.
[30] C.I. Liu, et al., A cholesterol biosynthesis inhibitor blocks Staphylococcus aureus virulence, Science 319 (5868) (2008) 1391–1394.
[31] B.R. Brooks, et al., CHARMM: the biomolecular simulation program, J. Comput. Chem. 30 (10) (2009) 1545–1614.
[32] S. Jo, et al., CHARMM-GUI PDB manipulator for advanced modeling and simulations of proteins containing nonstandard residues, Adv. Protein Chem. Struct. Biol. 96 (2014) 235–265.
[33] T. Tuccinardi, What is the current value of MM/PBSA and MM/GBSA methods in drug discovery? Expet Opin. Drug Discov. 16 (11) (2021) 1233–1237.
[34] C. Bouysset, S. Fiorucci, ProLIF: a library to encode molecular interactions as fingerprints, J. Cheminf. 13 (2021) 1–9.
[35] S. Salentin, et al., PLIP: fully automated protein–ligand interaction profiler, Nucleic Acids Res. 43 (W1) (2015) W443–W447.
[36] T. Tubiana, et al., TTClust: a versatile molecular simulation trajectory clustering program with graphical summaries, J. Chem. Inf. Model. 58 (11) (2018) 2178–2182.
[37] A. Amadei, et al., Essential dynamics of proteins, Proteins 17 (4) (1993) 412–425.
[38] E. Papaleo, et al., Free-energy landscape, principal component analysis, and structural clustering to identify representative conformations from molecular dynamics simulations: the myoglobin case, J. Mol. Graph. Model. 27 (8) (2009) 889–899.
[39] M. De Vivo, et al., Role of molecular dynamics and related methods in drug discovery, J. Med. Chem. 59 (9) (2016) 4035–4061.
[40] Z. Zhao, P.E. Bourne, Harnessing systematic protein-ligand interaction fingerprints for drug discovery, Drug Discov. Today 27 (10) (2022) 103319.
[41] S. Salentin, et al., From malaria to cancer: computational drug repositioning of amodiaquine using PLIP interaction patterns, Sci. Rep. 7 (1) (2017) 11401.
[42] N. Desdouits, et al., Principal Component Analysis reveals correlation of cavities evolution and functional motions in proteins, J. Mol. Graph. Model. 55 (2015) 13–24.
[43] H.B. Pinto, et al., The antivirulence compound myricetin possesses remarkable synergistic effect with antibacterials upon multidrug resistant Staphylococcus aureus, Microb. Pathog. 149 (2020) 104571.
[44] M. Iranshahi, et al., Protective effects of flavonoids against microbes and toxins: the cases of hesperidin and hesperetin, Life Sci. 137 (2015) 125–132.
[45] Q.H. Wen, et al., Inhibition of biofilm formation of foodborne Staphylococcus aureus by the citrus flavonoid naringenin, Foods 10 (11) (2021).
[46] L.A.A. Lopes, et al., Inhibitory effects of flavonoids on biofilm formation by Staphylococcus aureus that overexpresses efflux protein genes, Microb. Pathog. 107 (2017) 193–197.
[47] Y. Hu, et al., Silico prediction of human organ toxicity via artificial intelligence methods, Chem. Res. Toxicol. 36 (7) (2023) 1044–1054.